International Forum on Aeroelasticity and Structural Dynamics
IFASD 2024
17-21 June 2024, The Hague, The Netherlands

IDENTIFICATION OF FLEXIBLE AIRCRAFT PARAMETERS WITH VARYING FLEXIBILITY CONFIGURATIONS: INTEGRATING ELASTIC EFFECTS AND SENSOR DATA

Abraão Ferreira de Sousa Neto[1], **Kaique Silveira Viana Costa**[1], **Flávio Luiz Cardoso-Ribeiro**[*1]

[1]Instituto Tecnológico de Aeronáutica
Praça Marechal dos Campos, Brazil
[*]flaviocr@ita.br

Keywords: identification, flexible aircraft, output error method

Abstract: The necessity to mitigate pollutant emissions highlights the importance of research into flexible aircraft. Identifying models that accurately represent these aircraft is essential for the validation of early-stage design models and control design. This study focuses on performing a parametric system identification in the time domain for aircraft with varying levels of flexibility. The approach employs a simplified longitudinal stability and control model for short-period dynamics, rooted in the Quad-M methodology (Maneuver, Measurements, Model, and Method). The system identification technique used is the output error method, applied to a flexible model aircraft in three different flexibility configurations. Data were collected through nonlinear simulation of the flexible aircraft. Comparison of identification results across the different flexible configurations indicates an improvement in parametric values by incorporating elastic effects into the identification models. The study also explores the feasibility of various sensors to more closely simulate flight test procedures. Identifications are analyzed by comparing deflection measurements and accelerometers as observational variables, with acceleration measurements providing more accurate parameter estimations. Future work should extend the analysis presented to system identification using flight test data.

1 INTRODUCTION

Aviation faces various technological challenges, including reducing pollutant emissions. Consequently, aircraft with higher aspect ratios are now favored for their greater aerodynamic efficiency and lower fuel consumption. This trend raises concerns about flight dynamics, as vibrations from flexibility tend to occur at lower frequencies, leading to significant couplings that cannot be ignored.

Advances have been made in modeling, simulating, and testing flexible aircraft. At the Instituto Tecnológico de Aeronáutica (ITA), in partnership with the University of Michigan, the LNCA (Laboratory of New Concepts in Aeronautics) used the X-HALE prototype to study these aspects [1, 2]; see Figure 1. Validations and adjustments of these models are necessary, making system identification a crucial tool.

Aircraft identification theory has been thoroughly documented through two distinct approaches: in the time domain [3] and in the frequency domain [4]. While numerous studies focus on rigid-body aircraft identification, the identification of flexible aircraft remains less explored. A pioneering study by [5] discusses using the maximum likelihood method for parameter estimation

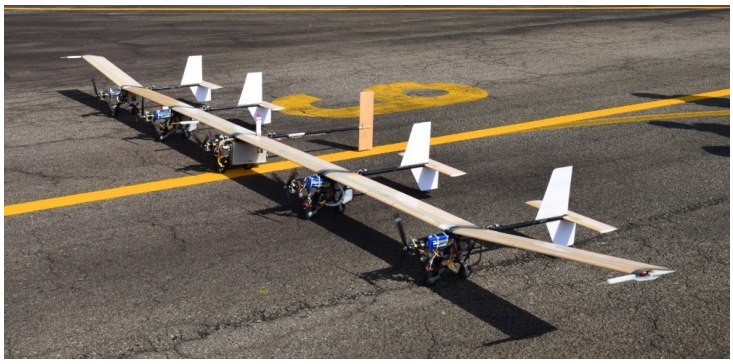

Figure 1: X-HALE prototype with a 6-meter wingspan from ITA/LNCA. Source: LNCA Internal Archive

in elastic aircraft, highlighting potential issues related to sensor placement, motion equation modeling, and center-of-mass positioning.

Transitioning from theoretical discussion to practical application, [6] conducted identification procedures for the Light Eagle, a highly flexible aircraft. Due to its low-frequency modes, significant coupling between elastic and rigid modes hindered successful identification. The study emphasized the need for a comprehensive elastic model and suitable maneuvers to excite elastic modes for accurate parameter identification.

More recent studies, such as [7], achieved complete aircraft identification in the time domain using the output error method, incorporating elastic effects and fluid-structure coupling in stability and control derivatives. This study validated the approach with five different modes and compared it with a rigid-body analysis. Similarly, [8] used the output error method with a reduced model, including elastic modes, angle of attack, and pitch rate, to characterize short-period dynamics' sensitivity to aircraft flexibility. Using a simulated platform, they identified desired stability and control derivatives. In the frequency domain, [9] successfully identified a dynamic model for a flying wing, considering three elastic modes and planning future control law design projects.

This work is motivated by the research conducted by [8], which used a simulated model with two elastic modes and fixed some derivatives to eliminate correlations. The analysis observed modal shapes, force in z, angle of attack, and pitch rate excited by a specific 3-2-1-1 maneuver. This work aims to improve upon previous research by not fixing any parameters and incorporating additional information from angular acceleration measurements and real sensors. The goal is to make the study procedure, conducted on simulated platforms, effective for future identification investigations on a real aircraft platform.

This paper is organized as follows: first, the simulation model is described in Section 2. Second, the model identification methodology is described in Section 3. Third, the airplane models and different flexibility configurations are presented in Section 4. Then, identification results are presented in Section 5. Finaly, conclusions and further work are discussed in Section 6.

2 FLEXIBLE AIRPLANE DYNAMICS - IDENTIFICATION AND SIMULATION MODEL

This work follows the equation of motion of flexible airplanes originally proposed by [10], where the following assumptions are considered:

- The structural deformation is sufficiently small, allowing the use of linear elastic theory;
- A set of normalized vibration modes is known (both frequency and modal shapes);

- Every mass element is point-like;
- The structural deformation is considered small, or simply that the deformation and its rate of change are collinear;
- The specific mass of each element is constant;
- The inertia tensor is considered constant.

Due to these hypotheses, the coupling between the rigid body equations of motion and the structural dynamic model occurs only due to the influence of the structural dynamics in the aerodynamics. Furthermore, the equations of motion are equivalent to classical rigid-body dynamics, added by second-order modal equations for the structural dynamics. The rigid body dynamics is given by:

$$\begin{aligned}
\dot{u} - rv + qw + g\sin\theta &= \frac{X}{m} \\
\dot{v} - pw + ru - g\sin\phi\cos\theta &= \frac{Y}{m} \\
\dot{w} - qu + pv - g\cos\phi\cos\theta &= \frac{Z}{m} \\
I_{xx}\dot{p} - (I_{xy}\dot{q} + I_{xz}\dot{r}) + (I_{zz} - I_{yy})qr + (I_{xy}r - I_{xz}q)p + (r^2 - q^2)I_{yz} &= \mathcal{L} \\
I_{yy}\dot{q} - (I_{xy}\dot{p} + I_{yz}\dot{r}) + (I_{xx} - I_{zz})pr + (I_{yz}p - I_{xy}r)q + (p^2 - r^2)I_{xz} &= \mathcal{M} \\
I_{zz}\dot{r} - (I_{xz}\dot{p} + I_{yz}\dot{q}) + (I_{yy} - I_{xx})pq + (I_{xz}q - I_{yz}p)r + (q^2 - p^2)I_{xy} &= \mathcal{N},
\end{aligned} \tag{1}$$

where the components of the aircraft's velocity in the body coordinate system are represented by (u, v, and w), the components of the angular velocity (p, q, and r), the Euler angles (ϕ, θ, and ψ), the moments and products of inertia of the aircraft (I_{xx}, I_{yy}, I_{zz}, I_{xy}, I_{xz}, I_{yz}), the aircraft's mass m, the altitude h, the forces in the X, Y, and Z axes, and the moments about the $\mathcal{L}$, $\mathcal{M}$, and $\mathcal{N}$ axes. To complete the state equations, the following kinematic relationships are added:

$$\begin{aligned}
\dot{\phi} &= p + q\sin\phi\tan\theta + r\cos\phi\tan\theta \\
\dot{\theta} &= q\cos\phi - r\sin\phi \\
\dot{\psi} &= (q\sin\phi + r\cos\phi)\sec\theta \\
\dot{h} &= u\sin\theta - v\sin\phi\cos\theta - w\cos\phi\cos\theta
\end{aligned} \tag{2}$$

In this formulation, the flexibility is considered by including modal coordinates degree of freedom, which leads to the following set of second-order equations:

$$\ddot{\eta}_i(t) + 2\xi_i\omega_{n_i}\dot{\eta}_i(t) + \omega_{n_i}^2\eta_i(t) = \frac{Q_i}{m_i}, \tag{3}$$

where η_i represents the modal displacements (displacements related to the i-th mode), Q_i the generalized forces acting on each mode, m_i the modal mass, ω_{n_i} the natural frequency, and ξ_i the damping factor. This development allows us to characterize the flexible aircraft with six degrees of freedom for the rigid body dynamics and an additional N degrees of freedom for the elastic modes, resulting in a total of $6 + N$ degrees of freedom.

The structural displacements can be recovered from the mode shapes ($\vec{\phi}_i(x, y, z)$) and the modal displacements ($\eta_i(t)$):

$$\vec{d} = \sum_{i=1}^{\infty} \vec{\phi}_i(x, y, z)\eta_i(t), . \tag{4}$$

This equation indicates that the displacement at each point is a linear combination of infinite mode shapes and modal displacements. For practical purposes, this sum is truncated, considering only a finite number (N) of known modal shapes. Typically, only low-frequency modes are considered, as they have a greater coupling with the traditional rigid body dynamics of the aircraft.

Finally, the aerodynamic forces, moments and generalized forces is obtained considering dimensionless coefficients:

$$\begin{aligned} X = q_\infty S C_X\,, \quad Y = q_\infty S C_Y\,, \quad Z = q_\infty S C_Z \\ \mathcal{M} = q_\infty S b C_\mathcal{M}\,, \quad \mathcal{L} = q_\infty S \bar{c} C_\mathcal{L}\,, \quad \mathcal{N} = q_\infty S b C_\mathcal{N}, \\ Q_i = q_\infty S C_{Q_i}\,, \end{aligned} \tag{5}$$

where the dimensionless coefficients are assumed linear with respect to flight variables, modal displacements and modal rates:

$$\begin{aligned} C_{X_F} &= C_0^{X_F} + C_\alpha^{X_F}\alpha + C_\beta^{X_F}\beta + C_\delta^{X_F}\delta + C_p^{X_F}p + C_q^{X_F}q + C_r^{X_F}r \\ &\quad + \sum_{i=1}^{N} C_{X_{\eta_i}}\eta_i + \sum_{i=1}^{N} C_{X_{\dot{\eta}_i}}\frac{\dot{\eta}_i\bar{c}}{2V} \\ C_{Y_F} &= C_0^{Y_F} + C_\alpha^{Y_F}\alpha + C_\beta^{Y_F}\beta + C_\delta^{Y_F}\delta + C_p^{Y_F}p + C_q^{Y_F}q + C_r^{Y_F}r \\ &\quad + \sum_{i=1}^{N} C_{Y_{\eta_i}}\eta_i + \sum_{i=1}^{N} C_{Y_{\dot{\eta}_i}}\frac{\dot{\eta}_i b}{2V} \\ C_{Z_F} &= C_0^{Z_F} + C_\alpha^{Z_F}\alpha + C_\beta^{Z_F}\beta + C_\delta^{Z_F}\delta + C_p^{Z_F}p + C_q^{Z_F}q + C_r^{Z_F}r \\ &\quad + \sum_{i=1}^{N} C_{Z_{\eta_i}}\eta_i + \sum_{i=1}^{N} C_{Z_{\dot{\eta}_i}}\frac{\dot{\eta}_i\bar{c}}{2V} \\ C_{\mathcal{L}_F} &= C_0^{\mathcal{L}F} + C_\alpha^{\mathcal{L}F}\alpha + C_\beta^{\mathcal{L}F}\beta + C_\delta^{\mathcal{L}_F}\delta + C_p^{\mathcal{L}_F}p + C_q^{\mathcal{L}_F}q + C_r^{\mathcal{L}_F}r \\ &\quad + \sum_{i=1}^{N} C_{\mathcal{L}_{\eta_i}}\eta_i + \sum_{i=1}^{N} C_{\mathcal{L}_{\dot{\eta}_i}}\frac{\dot{\eta}_i b}{2V} \\ C_{\mathcal{M}_F} &= C_0^{\mathcal{M}F} + C_\alpha^{\mathcal{M}F}\alpha + C_\beta^{\mathcal{M}F}\beta + C_\delta^{\mathcal{M}_F}\delta + C_p^{\mathcal{M}_F}p + C_q^{\mathcal{M}_F}q + C_r^{\mathcal{M}_F}r \\ &\quad + \sum_{i=1}^{N} C_{\mathcal{M}_{\eta_i}}\eta_i + \sum_{i=1}^{N} C_{\mathcal{M}_{\dot{\eta}_i}}\frac{\dot{\eta}_i\bar{c}}{2V} \\ C_{\mathcal{N}_F} &= C_0^{\mathcal{N}F} + C_\alpha^{\mathcal{N}F}\alpha + C_\beta^{\mathcal{N}F}\beta + C_\delta^{\mathcal{N}_F}\delta + C_p^{\mathcal{N}_F}p + C_q^{\mathcal{N}_F}q + C_r^{\mathcal{N}_F}r \\ &\quad + \sum_{i=1}^{N} C_{\mathcal{N}_{\eta_i}}\eta_i + \sum_{i=1}^{N} C_{\mathcal{N}_{\dot{\eta}_i}}\frac{\dot{\eta}_i b}{2V} \\ C_{Q_i} &= C_0^{\eta_i} + C_\alpha^{\eta_i}\alpha + C_\beta^{\eta_i}\beta + C_\delta^{\eta_i}\delta + C_p^{\eta_i}p + C_q^{\eta_i}q + C_r^{\eta_i}r \\ &\quad + \sum_{j=1}^{N} C_{\eta_j}^{\eta_i}\eta_j + \sum_{j=1}^{N} C_{\dot{\eta}_j}^{\eta_i}\frac{\dot{\eta}_j\bar{c}}{2V} \end{aligned} \tag{6}$$

The equations of motion for flexible vehicles under these hypotheses are closely related to the classical rigid body equations, assuming stability and control derivatives that typically have a clear physical meaning. These equations are particularly suitable for system identification, as the stability and control derivatives can be identified from flight tests.

In this preliminary work, the equations presented in this section will be used both to simulate the aircraft and to generate numerical data for evaluating the identification methodology. Furthermore, simplified versions of these equations will serve as the identification model.

3 MODEL IDENTIFICATION - QUAD-M METHODOLOGY

In this section, the system identification methodology to be used is presented. Based on Quad-M (presented by [3]), this section is subdivided into maneuver, measurements, model, and method, with the goal of describing the framework used for identification in this work.

3.1 Maneuver

Following the Quad-M standard, the first step consists of defining the Maneuver. The goal of identifying the stability derivatives related to a specific mode, whether it is rigid body dynamics or flexible, creates the need to perform a maneuver that excites this oscillatory movement.

The main maneuvers used in identification studies are step, pulse, doublet, 3-2-1-1 signal, and frequency sweep. The type of mode to be excited determines the choice of maneuvers to optimize the identification process of the necessary parameters. According to [3], the most common motions for system identification include exciting the short period, Dutch roll, phugoid, level turn, sideslip, pushover pullup, and bank-to-bank roll. Exciting the short period mode is particularly effective for identifying all derivatives related to the aircraft's longitudinal movement, making it the primary mode used in this work. To excite the short period mode, the doublet and 3-2-1-1 inputs are most commonly used. Ref. [3] provides an effective general rule for determining the time step of these inputs, as shown in:

$$\Delta t_{doublet} = \frac{2.3}{\omega_n} \tag{7}$$

$$\Delta t_{3211} = \frac{2.1}{\omega_n} \tag{8}$$

where ω_n is the natural frequency of the mode that should be excited.

In this work, we used doublet and 3-2-1-1 elevator inputs adjusted with the goal of exciting the short period mode and the first flexible natural frequencies of the airplane.

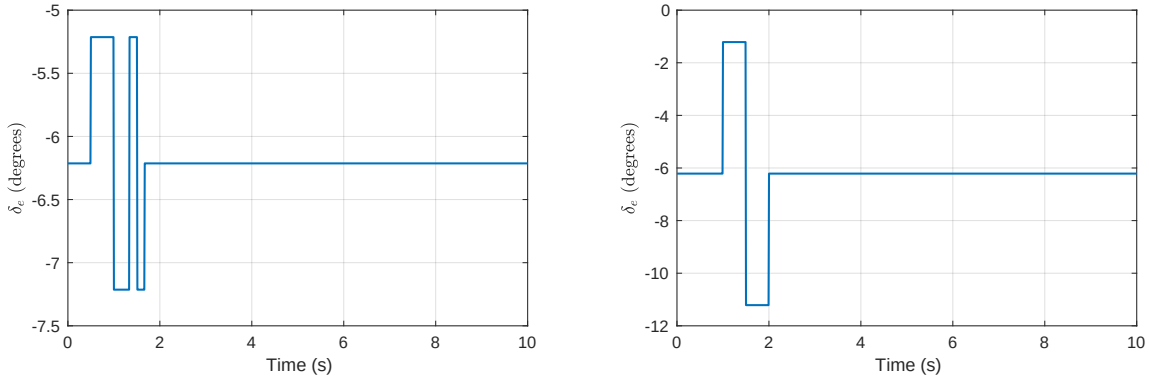

Figure 2: Example of maneuvers used for identification: 3-2-1-1 (left) and doublet (right).

3.2 Measurement

The measurements are related to the sensing design to obtain the necessary inputs and outputs for the identification process. In this preliminary study, we are preparing for future flight tests

that will be performed using our flexible aircraft platform, the ITA X-HALE. Meanwhile, simulation models were used to generate data, using a "virtual flight test". Different measurement strategies will be presented in the following sections. In all cases, the elevator control input, angle of attack and pitch rate will be measured. Furthermore, the following different choices will be explored in this work:

1. Measuring of modal displacements (η_i) and their rates ($\dot{\eta}_i$) (which is a purely theoretical test of the methodology, since we wouldn't be able measure these variables directly in a flight test);
2. Measuring structural displacements at different points of the flexible structure;
3. Measuring accelerations at different points of the flexible structure;
4. Furthermore, some simulations will also consider measuring the total forces and moments applied to the airplane (or, vertical acceleration of the rigid-body, and angular acceleration).

3.3 Model

In this work, the focus will be on parametric identification in the time domain, considering a simplified model of the one presented in Section 2.

Only the short-period dynamics will be considered among the rigid-body degrees of freedom. In this case, the state variables will be the vertical component of the aircraft's velocity in the body axis w and the pitch rate q, in addition to the elastic modes. The dynamic equations are represented by:

$$\dot{w} = (qum + mg\cos\theta + Q_z)/m, \tag{9}$$

$$\dot{q} = Q_M/I_{yy}, \tag{10}$$

$$\ddot{\eta}_i = -2\xi_i\omega_{n_i}\dot{\eta}_i - \omega_{n_i}^2\eta_i + \frac{Q_{\eta_i}}{m_i} \tag{11}$$

where Q_z and Q_M represent the vertical force and pitching moment, respectively:

$$Q_z = \frac{1}{2}\rho\bar{c}V_0^2S\left(C_{Z0} + C_{Z\alpha}\alpha + C_{Z\delta}\delta + \sum_{i=1}^{\infty}C_{Z\eta_i}\eta_i\right) + \frac{1}{4}\rho\bar{c}^2V_0S\left(C_{Zq}q + \sum_{i=1}^{\infty}C_{Z\dot{\eta}_i}\dot{\eta}_i\right), \tag{12}$$

$$Q_M = \frac{1}{2}\rho\bar{c}V_0^2S\left(C_{M0} + C_{M\alpha}\alpha + C_{M\delta}\delta + \sum_{i=1}^{\infty}C_{M\eta_i}\eta_i\right) + \frac{1}{4}\rho\bar{c}^2V_0S\left(C_{Mq}q + \sum_{i=1}^{\infty}C_{M\dot{\eta}_i}\dot{\eta}_i\right). \tag{13}$$

For the identification model, all the mass and structural information is supposed to be known, and we will focus on identifying the aerodynamic stability and control derivatives.

During this work different hypotheses about the number of modes of the identification model will be considered (including a case of a rigid body only, with $N = 0$).

3.4 Method

The method represents the identification procedure itself that will be used. In this work, the focus was on time domain identification, exploring the output error method.

The output error method consists of a parametric prediction of a mathematical model through the minimization of a cost function between the predicted model and the data received from the

system. To perform the estimation, Ref. [3] uses Fisher's maximum likelihood theory:

$$J(\Theta, R) = \frac{1}{2}\sum_{k=1}^{N}[z(t_k) - y(t_k)]^T R^{-1}[z(t_k) - y(t_k)] + \frac{N}{2}ln[det(R)] + \frac{Nn_y}{2}ln(2\pi), \quad (14)$$

where z represents the measured data vector, y is the model output vector, t_k is the sampling time, n_y the number of observation variables, Θ the parameter vector, and R is the measurement noise covariance matrix, which is generally unknown in flight tests. Since simulated data were used in this work to replace the tests, the disturbances applied to each data point are known, and thus the cost function reduces to the following equation, as the other terms are constants:

$$J(\Theta, R) = \frac{1}{2}\sum_{k=1}^{N}[z(t_k) - y(t_k)]^T R^{-1}[z(t_k) - y(t_k)] \quad (15)$$

The minimum of the cost function is obtained by $\frac{\partial J(\Theta,R)}{\partial \Theta} = 0$. Expanding in a Taylor series and truncating after the first term, we have:

$$\frac{\partial J(\Theta, R)}{\partial \Theta}_{i+1} \approx \frac{\partial J(\Theta, R)}{\partial \Theta}_{i} + \frac{\partial^2 J(\Theta, R)}{\partial \Theta^2}_{i}\Delta\Theta, \quad (16)$$

where $\Delta\Theta = \Theta_{i+1} - \Theta_i$. Since the first derivative is zero, and inverting the Hessian matrix to isolate the parameter vector, we have:

$$\Delta\Theta = -\left[\frac{\partial^2 J(\Theta, R)}{\partial \Theta^2}_{i}\right]^{-1}\frac{\partial J(\Theta, R)}{\partial \Theta}_{i}. \quad (17)$$

The complexity of this method is related to obtaining the Hessian matrix. Ref. [3] presents Balakrishnan's simplification which applied leads to the optimization methodology known as Gauss-Newton. Another method, Levenberg-Marquardt, combines gradient descent with Gauss-Newton, increasing the convergence region of the method, implemented in this work. Basically, an update parameter is introduced in the Hessian matrix, exemplified in:

$$\frac{\partial^2 J(\Theta, R)}{\partial \Theta^2} = \sum_{k=1}^{N}\left[\frac{\partial y(t_k)}{\partial \Theta}\right]^T R^{-1}\left[\frac{\partial y(t_k)}{\partial \Theta}\right]. \quad (18)$$

In this work, the Levenberg-Marquardt is used as optimization method.

4 FLEXIBLE AIRCRAFT SIMULATION MODEL

This section describes the simulation model used in this paper, based on the equatins presented in Section 2. The aircraft is based on the model described by [10], which is similar to the B1-Lancer airplane (Fig. 3). The geometric and inertia properties of the model are presented in Table 1 and stability and control derivatives are presented in Table 2.

The original study considered three different configurations: C1 (rigid aircraft), C2 (baseline flexible aircraft) and C3 (more flexible aircraft). We defined a C4 configuration, even more flexible. The difference between each configuration is basically the in vacuo vibration frequencies, which are detailed in Table 3.

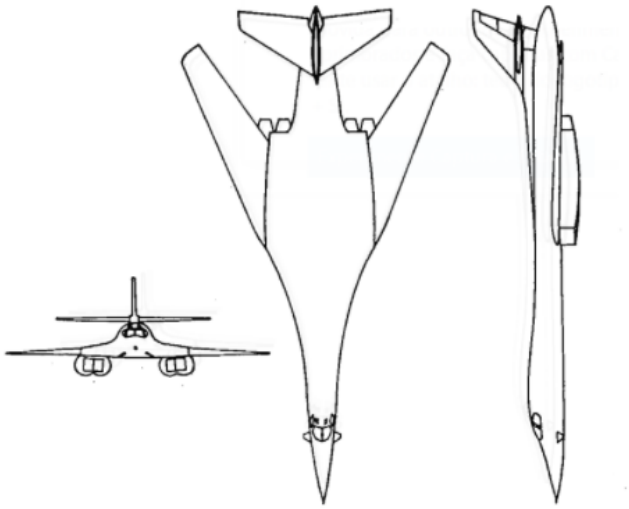

Figure 3: Flexible aircraft model. Source: [10]

Table 1: Aircraft properties. Source: 10

Property	Variable	Value	Unit
Geometry	$\bar{c}$	4.66344	m
	b	21.34	m
	S	180.79	m^2
Weight	W	130642	kg
Inertia	I_{yy}	8677234.88	$kg.m^2$
Modal Masses	m_1	248.93	$kg.m^2$
	m_2	12997.55	$kg.m^2$

Table 2: Stability and control derivatives presented by [10]

Q_x		Q_z		Q_M		Q_{η_1}		Q_{η_2}	
C_{X0}	-0.028	C_{Z0}	-0.34	C_{M0}	-0.252	$C_0^{\eta_1}$	0.0	$C_0^{\eta_2}$	0.0
C_{X_α}	0.035	C_{Z_α}	-0.051	C_{M_α}	-0.029	$C_\alpha^{\eta_1}$	-2.6e-04	$C_\alpha^{\eta_2}$	4.5e-04
C_{X_q}	-1.7	C_{Z_q}	14.7	C_{M_q}	-34.75	$C_q^{\eta_1}$	-9.49e-02	$C_q^{\eta_2}$	1.16e-02
C_{X_δ}	0.0267	C_{Z_δ}	-0.0076	C_{M_δ}	-0.045	$C_\delta^{\eta_1}$	-2.24e-04	$C_\delta^{\eta_2}$	-1.12e-03
$C_{X_{\eta_1}}$	0.0	$C_{Z_{\eta_1}}$	-0.0288	$C_{M_{\eta_1}}$	-0.0321	$C_{\eta_1}^{\eta_1}$	5.85e-05	$C_{\eta_2}^{\eta_1}$	4.21e-03
$C_{X_{\dot{\eta}_1}}$	0.0	$C_{Z_{\dot{\eta}_1}}$	-0.0848	$C_{M_{\dot{\eta}_1}}$	-0.159	$C_{\dot{\eta}_1}^{\eta_1}$	-4.2e-04	$C_{\dot{\eta}_2}^{\eta_1}$	8.71e-03
$C_{X_{\eta_2}}$	0.0	$C_{Z_{\eta_2}}$	0.306	$C_{M_{\eta_2}}$	-0.025	$C_{\eta_1}^{\eta_2}$	-9.0e-05	$C_{\eta_2}^{\eta_2}$	-9.22e-02
$C_{X_{\dot{\eta}_2}}$	0.0	$C_{Z_{\dot{\eta}_2}}$	1.03	$C_{M_{\dot{\eta}_2}}$	1.23	$C_{\dot{\eta}_1}^{\eta_2}$	-1.97e-04	$C_{\dot{\eta}_2}^{\eta_2}$	-2.98e-01

Table 3: In vacuo modal vibration frequencies. Source: 10.

	Frequency $[rad/s]$	
Configuration	Mode 1	Mode 2
$C1$ (rigid)	-	-
$C2$ (baseline)	12.57	14.07
$C3$	6.29	7.04
$C4$	3.14	3.52

With the necessary data collection in hand, simulations are fed with a 3-2-1-1 maneuver applied to the elevator, as depicted in Figure 4. The response of angle of attack and pitch rate, for each of the four configurations, are presented in Figures 5 and 6, respectively. The responses for the C2 configuration are very similar to those of the rigid body (C1) model. Small differences are observed in the C3 model. On the other hand, the C4 model response is largely modified (since the in vacuo vibration modes are closer to the rigid body short period mode). In the sequel, we will use these different configuration models to test the output error method for identification purposes under different hypothesis. Since the baseline C2 is only slightly flexible (and the flexible dynamics does not considerably affects the rigid-body variables, we decided to focus the following study in the C3 and C4 configurations).

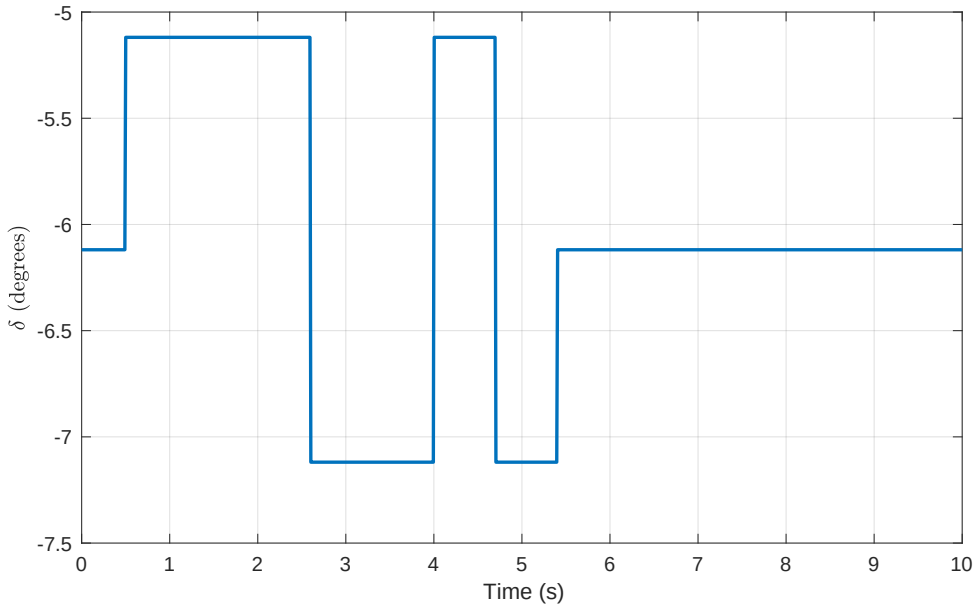

Figure 4: Input of elevator used in the simulation (3-2-1-1)

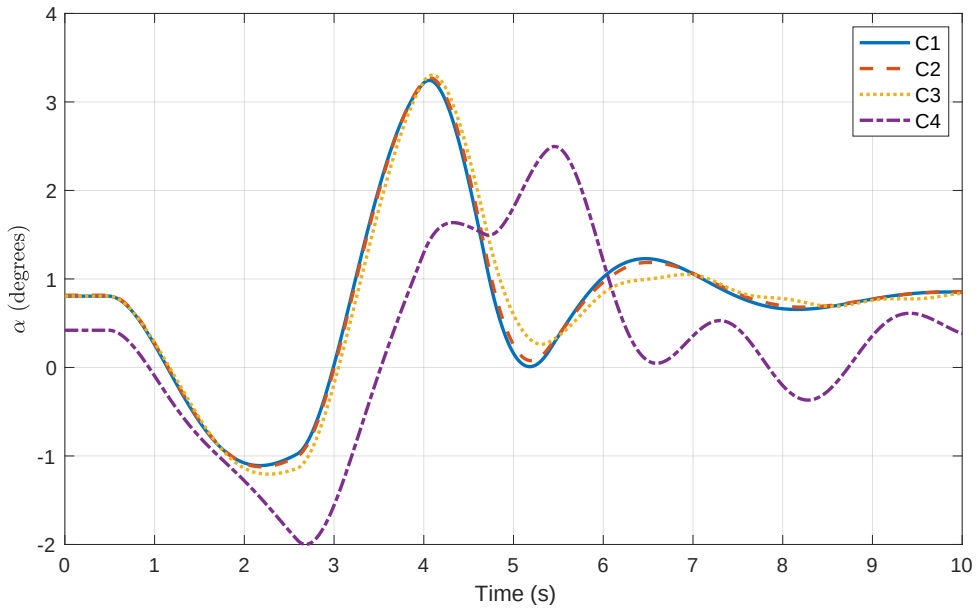

Figure 5: Angle of attack response for the same inputs considering the different configurations (aircraft flexibilities)

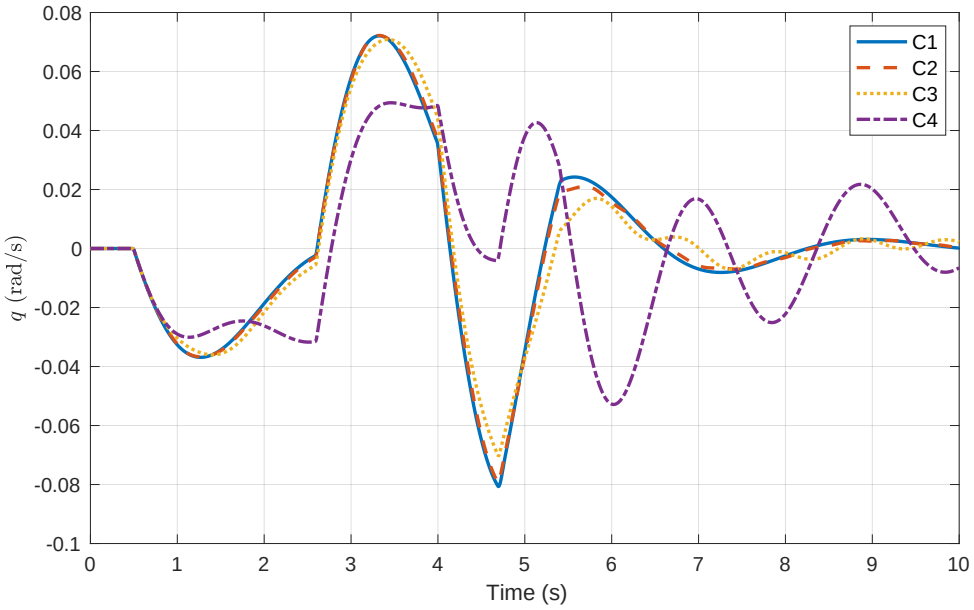

Figure 6: Pitch rate response for the same inputs considering the different configurations (aircraft flexibilities)

5 IDENTIFICATION RESULTS CONSIDERING THE C1, C3 AND C4 CONFIGURATIONS

This section is organized as follows. Firstly, rigid body (C1) is used both as simulation and identification model (considering only short-period dynamics in the case of identification model) in § 5.1. Secondly, C3 aircraft is used as simulation model, and three simplified models are used for identification: rigid-body short-period, 1 mode, and 2 modes model coupled with short-period dynamics in § 5.2. Thirdly, the same analysis is repeated for the C4 configuration in § 5.3. Then, rigid-body force and moment are added as measured outputs in § 5.4. Finally, displacement and acceleration measurements are considered as sensors in § 5.5.

5.1 Rigid body (C1) as simulation model

Our first test was simply considering that both the simulation and the identification model uses only the rigid body degrees of freedom. The only difference between those models is that the simulation model considers all the longitudinal states, and the identification model assumes only the short-period states. This is a very classical identification problem, results for the identification of stability derivatives are presented in Table 7, and the simulation results are presented in Figure 8. A sequence of 3-2-1-1 and a doublet maneuver as performed to generate the identification data from the simulation model. The output error method was able to identify most stability derivatives with small error.

Table 4: Comparison of Nominal and Identified Parameters - RB as identification and simulation model

Parameter	Nominal Value	Identified Value	Percentual Error (%)
C_{z0}	-0.3400	-0.3447	1.40
C_{z_α}	-2.9221	-2.9176	-0.15
C_{z_q}	14.7000	13.1937	-10.25
$C_{z_{\delta_e}}$	-0.0076	-0.0083	9.74
C_{m_0}	-0.2520	-0.2551	1.25
C_{m_α}	-1.6616	-1.6737	0.73
C_{m_q}	-34.7500	-34.9339	0.53
$C_{m_{\delta_e}}$	-0.0450	-0.0455	1.18

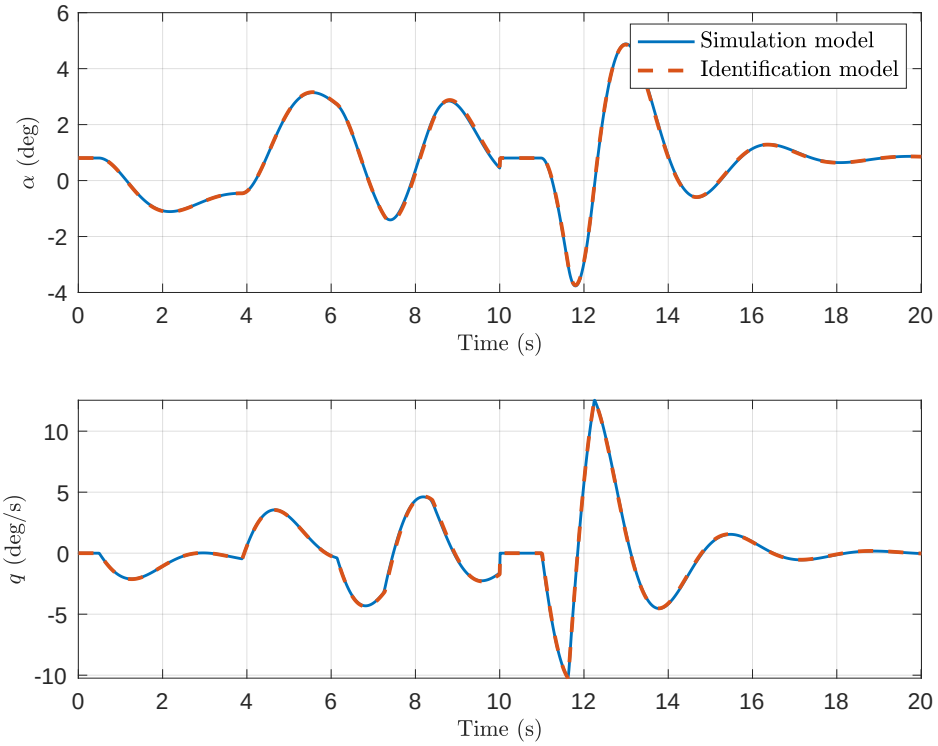

Figure 7: C1 rigid body model as simulation model, rigid body as identification model

5.2 C3 flexible aircraft as simulation model

Secondly, we performed several tests considering the C3 flexible aircraft as simulation model. We increased the complexity of the identification model as follows: First, we assumed only the rigid-body model; Second, we assumed the identification model with only one flexible mode. Finally, two flexible modes were considered in the identification model.

The results for the rigid-body identification model are presented in Table 5 and Figure 8. Despite the very good agreement between the responses, the errors related to the stability derivatives are much larger (most of them larger than 10%). The 1-mode and 2-mode identification models also exhibit very good agreement in the responses, as appears in Figures 9,10,11 and 12. From Tables 6 and 7, some improvement is observed in the rigid body stability derivatives (despite the large errors in C_{z_q} and C_{z_δ}). Most modal-related stability derivatives have errors smaller than 10%, with the notorious exception of those related to the coupling effect of η_1 and η_2 (and vice versa), such as $C_{\eta_1\eta_2}$ and $C_{\eta_1\dot{\eta}_2}$ which exhibit errors of about 250% and 640%, respectively.

Table 5: Comparison of Nominal and Identified Parameters - RB identification model - C3 simulation model

Parameter	Nominal Value	Identified Value	Percentual Error (%)
C_{z0}	-0.3400	-0.3464	1.90
C_{z_α}	-2.9221	-2.7420	-6.16
C_{z_q}	14.7000	19.9934	36.01
$C_{z_{\delta_e}}$	-0.0076	-0.0076	0.43
C_{m_0}	-0.2520	-0.2426	-3.74
C_{m_α}	-1.6616	-1.4448	-13.04
C_{m_q}	-34.7500	-31.0332	-10.70
$C_{m_{\delta_e}}$	-0.0450	-0.0405	-10.02

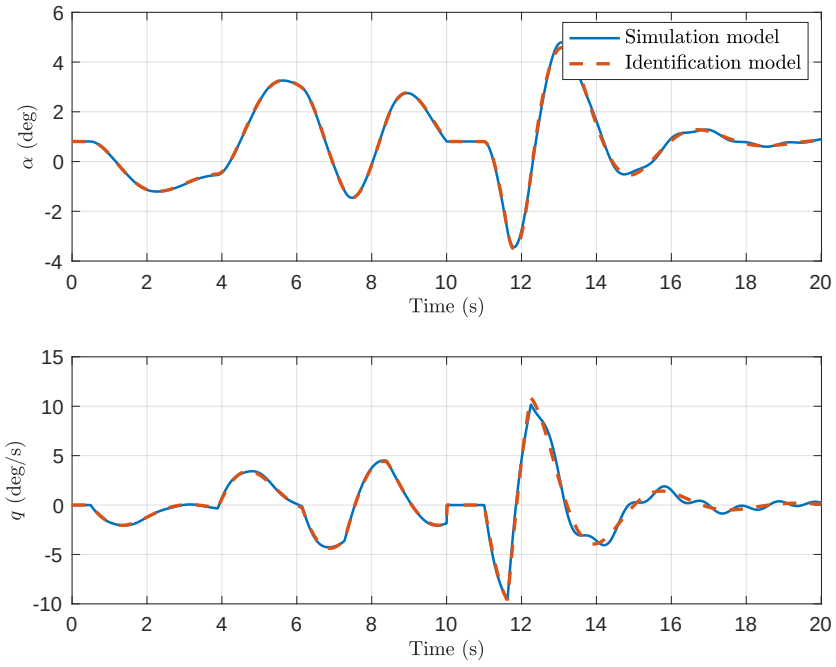

Figure 8: Flexible model as simulation model, rigid body as identification model

Table 6: Comparison of Nominal and Identified Parameters - C3 as simulation model - 1 mode identification model

Parameter	Nominal Value	Identified Value	Percentual Error (%)
C_{z0}	-0.3400	-0.3500	2.95
C_{z_α}	-2.9221	-2.8260	-3.29
C_{z_q}	14.7000	11.5565	-21.38
$C_{z_{\delta_e}}$	-0.0076	-0.0098	29.46
C_{m_0}	-0.2520	-0.2511	-0.35
C_{m_α}	-1.6616	-1.6634	0.11
C_{m_q}	-34.7500	-33.2419	-4.34
$C_{m_{\delta_e}}$	-0.0450	-0.0448	-0.43
$C_{\eta_{1\alpha}}$	-0.0149	-0.0150	1.00
$C_{\eta_{1\delta}}$	-0.0002	-0.0002	-0.17
$C_{z_{\eta_1}}$	-0.0288	-0.0180	-37.38
$C_{z_{\dot{\eta_1}}}$	-0.0848	-0.0586	-30.89
$C_{m_{\eta_1}}$	-0.0321	-0.0333	3.73
$C_{m_{\dot{\eta_1}}}$	-0.1590	-0.1143	-28.12
$C_{\eta_{1q}}$	-0.0949	-0.0868	-8.55
$C_{\eta_{1\eta_1}}$	0.0001	0.0001	-2.97
$C_{\eta_{1\dot{\eta_1}}}$	-0.0004	-0.0004	3.96

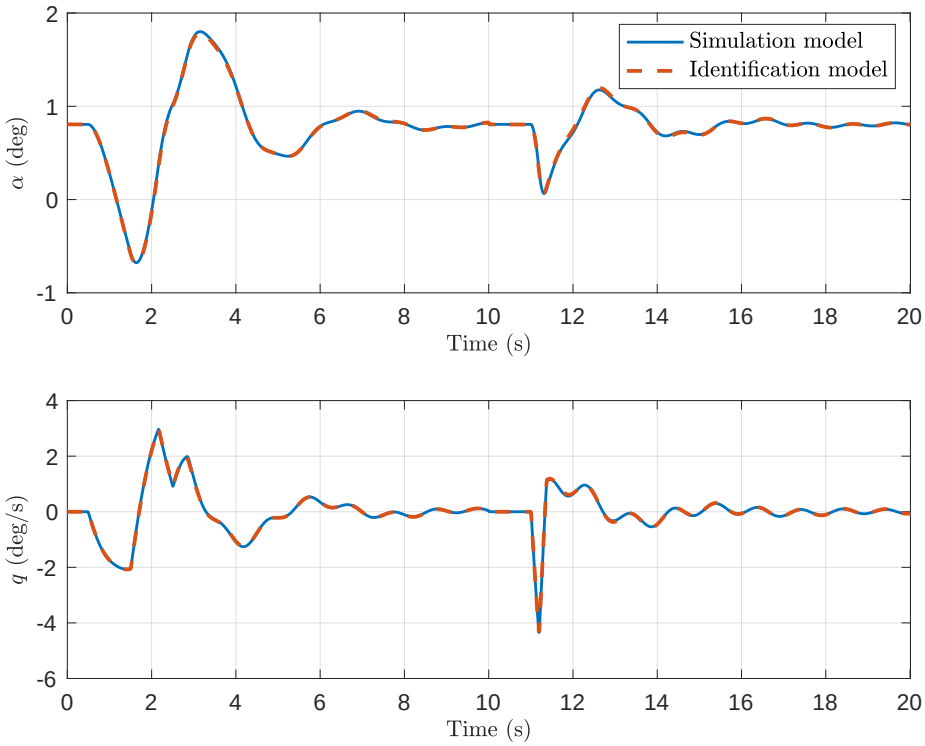

Figure 9: Flexible model as simulation model, flexible aircraft with one mode as identification model

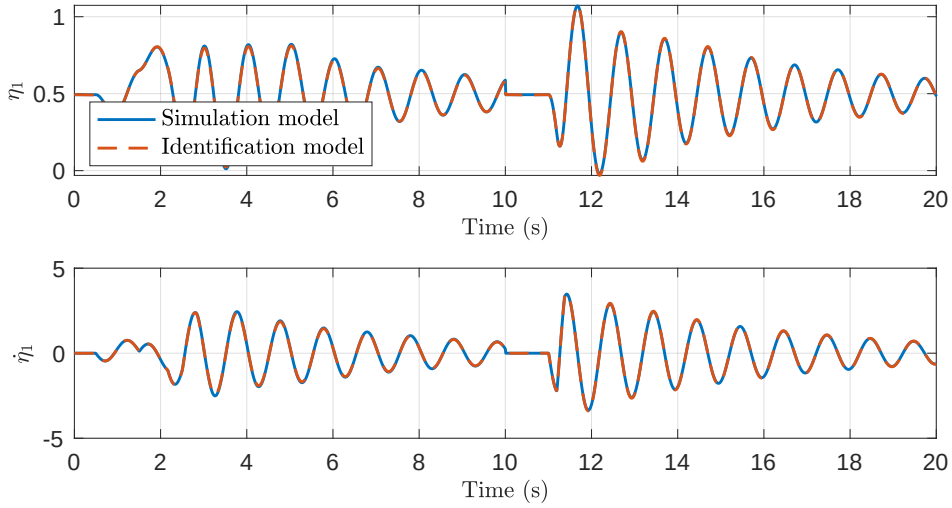

Figure 10: Flexible model as simulation model, flexible aircraft with one mode as identification model - modal displacements

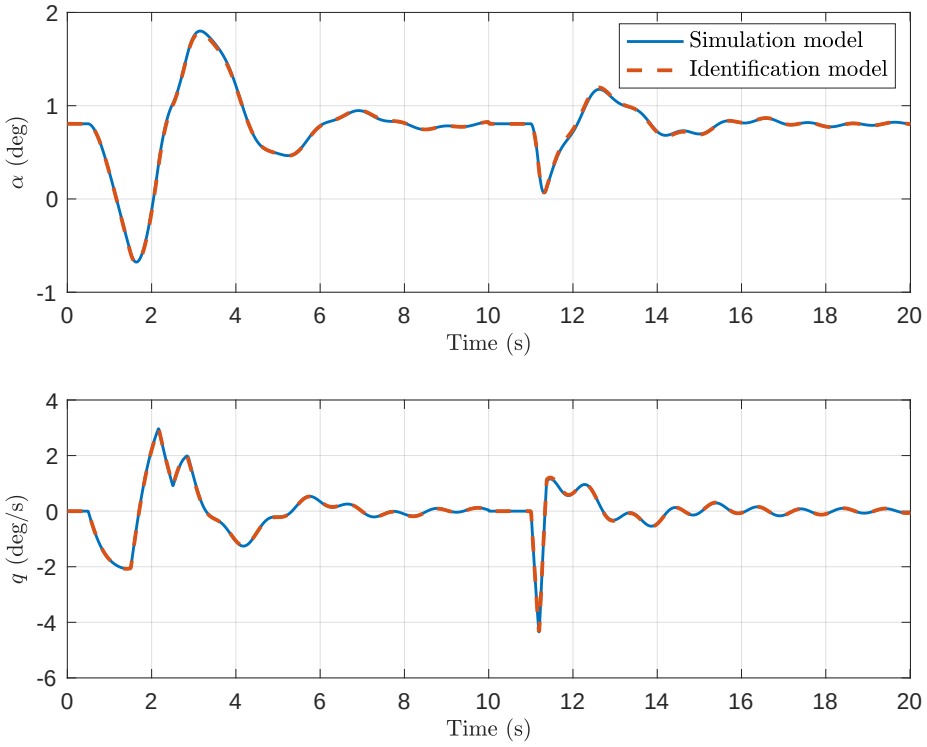

Figure 11: Flexible model as simulation model, flexible aircraft with one two modes as identification model

Table 7: Comparison of Nominal and Identified Parameters - C3 as simulation model - 2 modes identification model

Parameter	Nominal Value	Identified Value	Percentual Error (%)
C_{z0}	-0.3400	-0.3502	2.99
C_{z_α}	-2.9221	-2.9290	0.24
C_{z_q}	14.7000	11.6300	-20.88
$C_{z_{\delta_e}}$	-0.0076	-0.0089	17.40
C_{m_0}	-0.2520	-0.2500	-0.80
C_{m_α}	-1.6616	-1.6552	-0.39
C_{m_q}	-34.7500	-33.2620	-4.28
$C_{m_{\delta_e}}$	-0.0450	-0.0446	-0.89
$C_{\eta_{1\,\alpha}}$	-0.0149	-0.0152	1.70
$C_{\eta_{1\,\delta}}$	-0.0002	-0.0002	-0.38
$C_{z_{\eta_1}}$	-0.0288	-0.0319	10.78
$C_{z_{\dot{\eta_1}}}$	-0.0848	-0.0485	-42.84
$C_{m_{\eta_1}}$	-0.0321	-0.0324	1.05
$C_{m_{\dot{\eta_1}}}$	-0.1590	-0.1529	-3.81
$C_{\eta_{1\,q}}$	-0.0949	-0.0885	-6.70
$C_{\eta_{1\,\eta_1}}$	0.0001	0.0001	-11.61
$C_{\eta_{1\,\dot{\eta_1}}}$	-0.0004	-0.0004	-7.84
$C_{\eta_{1\,\eta_2}}$	-0.0001	0.0001	-248.70
$C_{\eta_{2\,\eta_1}}$	0.0042	0.0042	-0.19
$C_{\eta_{2\,\eta_2}}$	-0.0922	-0.0916	-0.70
$C_{\eta_{1\,\dot{\eta_2}}}$	-0.0002	-0.0015	641.75
$C_{\eta_{2\,\dot{\eta_1}}}$	0.0087	0.0089	1.82
$C_{\eta_{2\,\dot{\eta_2}}}$	-0.2980	-0.3009	0.97
$C_{\eta_{2\,\alpha}}$	0.0258	0.0268	3.87
$C_{\eta_{2\,q}}$	0.0116	0.0316	172.66
$C_{\eta_{2\,\delta}}$	-0.0011	-0.0011	-0.26
$C_{z_{\eta_2}}$	0.3060	0.3842	25.56
$C_{z_{\dot{\eta_2}}}$	1.0300	-0.8270	-180.29
$C_{m_{\eta_2}}$	-0.0250	-0.0097	-61.23
$C_{m_{\dot{\eta_2}}}$	1.2300	1.1827	-3.84

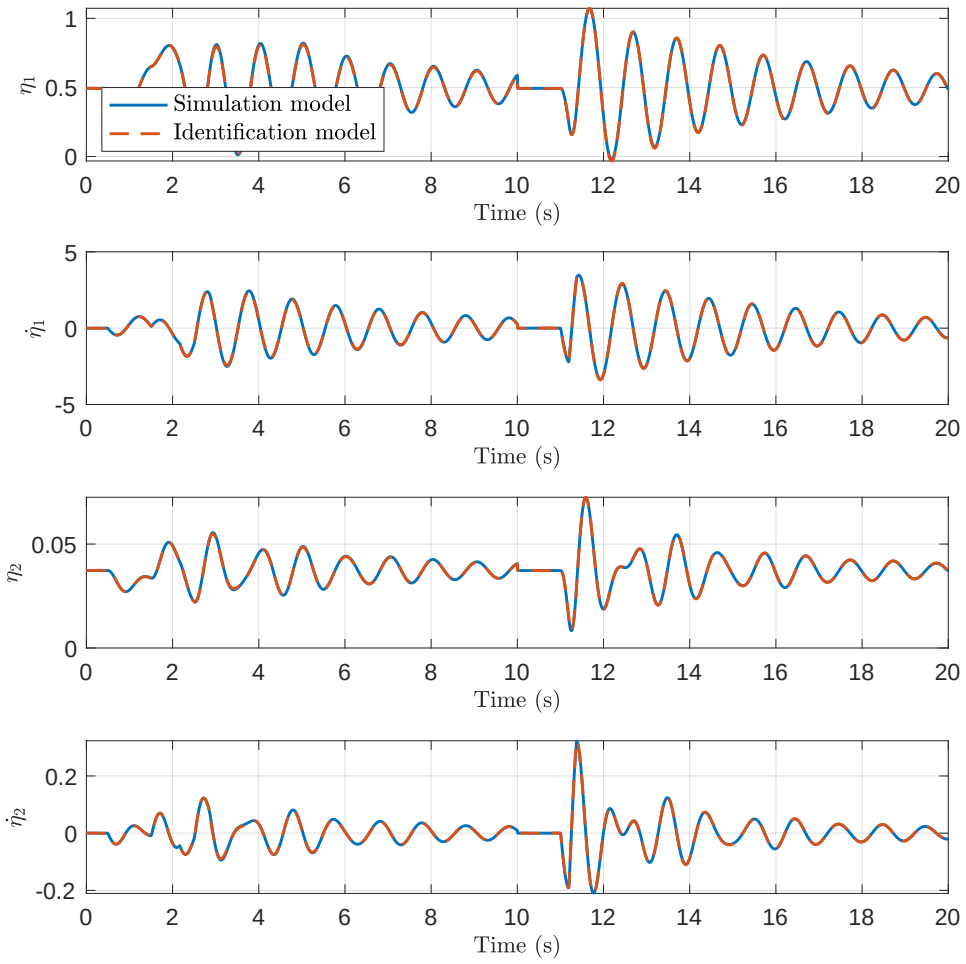

Figure 12: Flexible model as simulation model, flexible aircraft with one two modes as identification model - modal displacements

5.3 C4 - very flexible aircraft simulation model

In this subsection, we performed several tests considering the C4 very flexible aircraft as simulation model. As in the previous subsection, we increased the complexity of the identification model as follows: First, we assumed only the rigid-body model; Second, we assumed the identification model with only one flexible mode. Finally, two flexible modes were considered in the identification model.

The results for the rigid-body identification model are presented in Table 8 and Figure 13. Differently from model C3, the responses are not adequately repeated using the rigid body identification model for the very flexible C4 model. The errors related to the stability derivatives are even larger than in previous results. Adding at least one mode to the identification model, significantly improves the matching of identified-model response as seem in Figures 14,15,16 and 17. From Tables 9 and 10, the errors in the identified stability derivatives are similar to those obtained in the C3 model.

Table 8: Comparison of Nominal and Identified Parameters - C4 as simulation model - rigid body as identification model

Parameter	Nominal Value	Identified Value	Percentual Error (%)
C_{z0}	-0.3400	-0.8619	153.50
C_{z_α}	-2.9221	-2.0223	-30.79
C_{z_q}	14.7000	-117.5717	-899.81
$C_{z_{\delta_e}}$	-0.0076	-0.0680	794.94
C_{m_0}	-0.2520	-0.1694	-32.76
C_{m_α}	-1.6616	-0.7057	-57.53
C_{m_q}	-34.7500	-16.0994	-53.67
$C_{m_{\delta_e}}$	-0.0450	-0.0218	-51.61

Table 9: Comparison of Nominal and Identified Parameters - C4 as simulation model - 1 mode identification model

Parameter	Nominal Value	Identified Value	Percentual Error (%)
C_{z0}	-0.3400	-0.3704	8.95
C_{z_α}	-2.9221	-2.7365	-6.35
C_{z_q}	14.7000	5.6958	-61.25
$C_{z_{\delta_e}}$	-0.0076	-0.0128	67.95
C_{m_0}	-0.2520	-0.2550	1.19
C_{m_α}	-1.6616	-1.7080	2.79
C_{m_q}	-34.7500	-36.3258	4.53
$C_{m_{\delta_e}}$	-0.0450	-0.0455	1.11
$C_{\eta_{1\alpha}}$	-0.0149	-0.0152	1.80
$C_{\eta_{1\delta}}$	-0.0002	-0.0002	0.31
$C_{z_{\eta_1}}$	-0.0288	-0.0162	-43.59
$C_{z_{\dot{\eta_1}}}$	-0.0848	-0.0801	-5.54
$C_{m_{\eta_1}}$	-0.0321	-0.0338	5.17
$C_{m_{\dot{\eta_1}}}$	-0.1590	-0.0965	-39.28
$C_{\eta_{1q}}$	-0.0949	-0.1058	11.52
$C_{\eta_{1\eta_1}}$	0.0001	0.0001	-9.96
$C_{\eta_{1\dot{\eta_1}}}$	-0.0004	-0.0003	-23.48

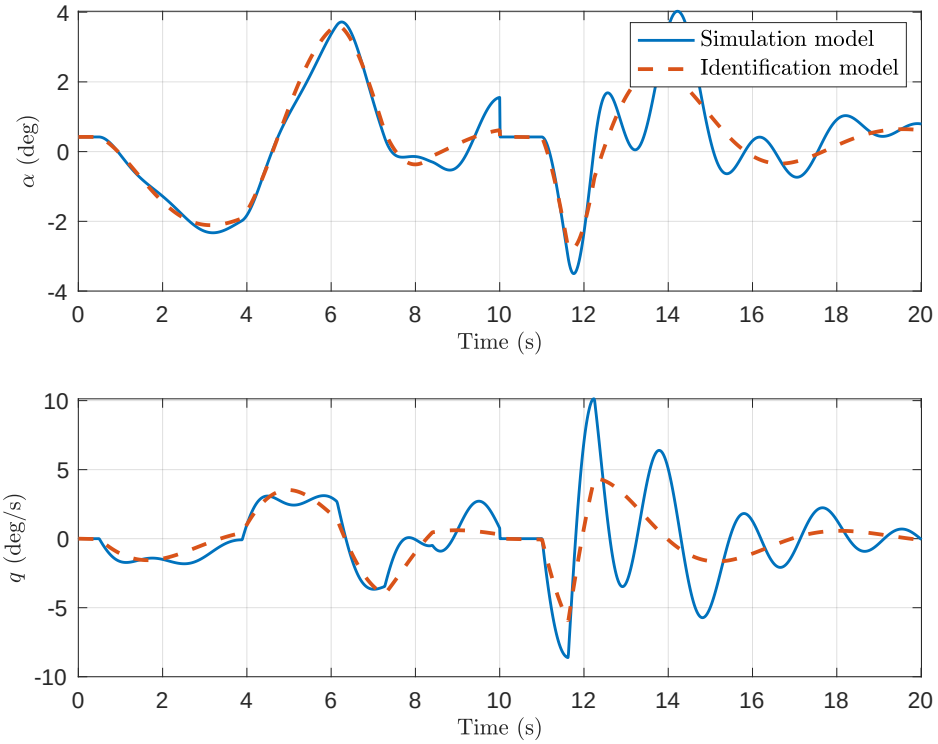

Figure 13: Very flexible model as simulation model, rigid body as identification model

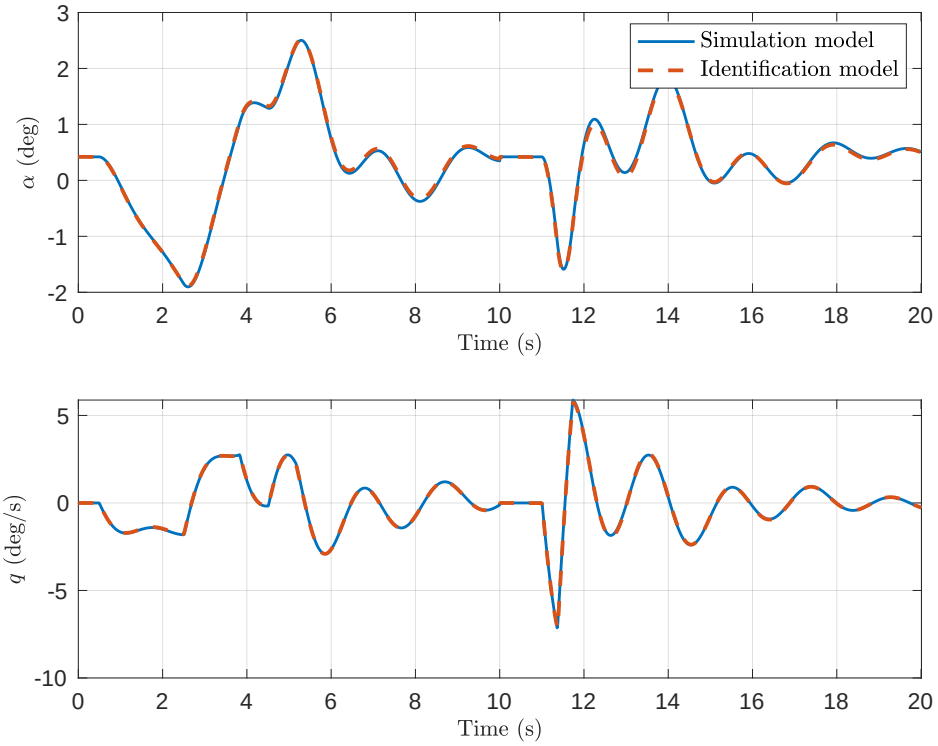

Figure 14: Very flexible model as simulation model, flexible aircraft with 1 mode as identification model

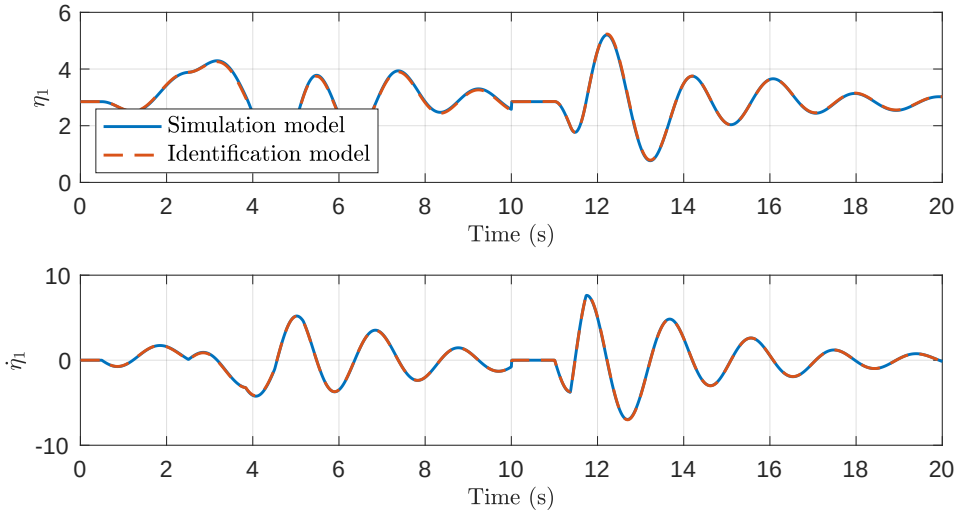

Figure 15: Very flexible model as simulation model, flexible aircraft with 1 mode as identification model - modal displacements

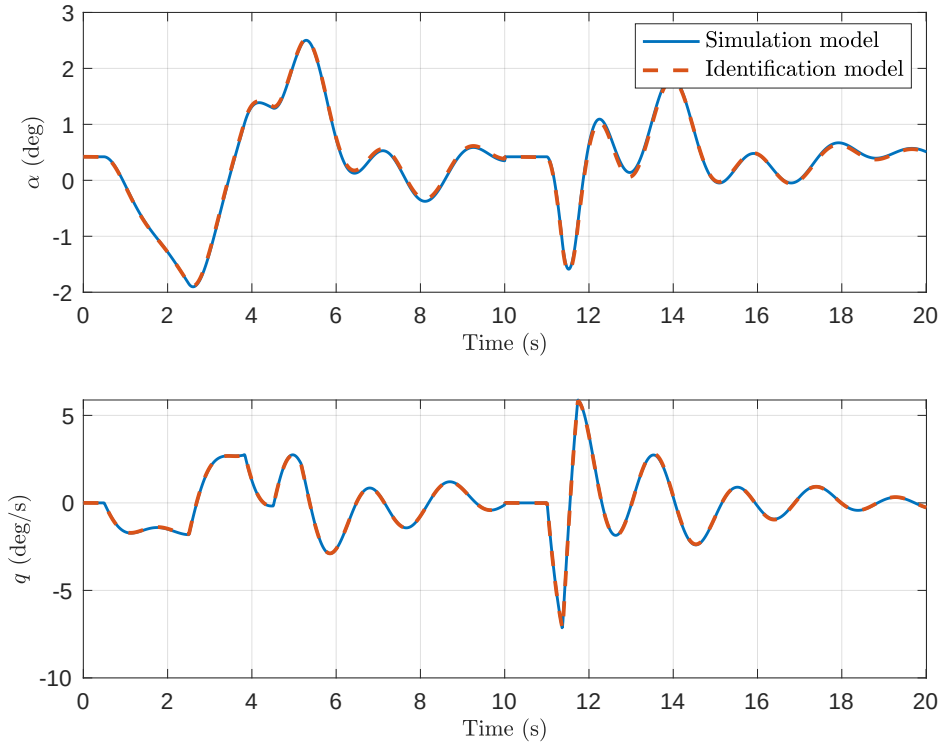

Figure 16: Very flexible model as simulation model, flexible aircraft with 2 modes as identification model

Table 10: Comparison of Nominal and Identified Parameters - C4 as simulation model - 2 modes identification model

Parameter	Nominal Value	Identified Value	Percentual Error (%)
C_{z0}	-0.3400	-0.3717	9.34
C_{z_α}	-2.9221	-2.9893	2.30
C_{z_q}	14.7000	8.8777	-39.61
$C_{z_{\delta_e}}$	-0.0076	-0.0114	49.68
C_{m_0}	-0.2520	-0.2531	0.42
C_{m_α}	-1.6616	-1.6660	0.26
C_{m_q}	-34.7500	-35.9466	3.44
$C_{m_{\delta_e}}$	-0.0450	-0.0454	0.98
$C_{\eta_{1\,\alpha}}$	-0.0149	-0.0150	0.51
$C_{\eta_{1\,\delta}}$	-0.0002	-0.0002	0.99
$C_{z_{\eta_1}}$	-0.0288	-0.0335	16.48
$C_{z_{\dot{\eta_1}}}$	-0.0848	0.1257	-248.19
$C_{m_{\eta_1}}$	-0.0321	-0.0306	-4.71
$C_{m_{\dot{\eta_1}}}$	-0.1590	-0.1349	-15.14
$C_{\eta_{1\,q}}$	-0.0949	-0.1003	5.70
$C_{\eta_{1\,\eta_1}}$	0.0001	0.0001	24.18
$C_{\eta_{1\,\dot{\eta_1}}}$	-0.0004	-0.0003	-27.33
$C_{\eta_{1\,\eta_2}}$	-0.0001	-0.0005	407.74
$C_{\eta_{2\,\eta_1}}$	0.0042	0.0042	0.27
$C_{\eta_{2\,\eta_2}}$	-0.0922	-0.0928	0.65
$C_{\eta_{1\,\dot{\eta_2}}}$	-0.0002	-0.0011	480.56
$C_{\eta_{2\,\dot{\eta_1}}}$	0.0087	0.0096	9.79
$C_{\eta_{2\,\dot{\eta_2}}}$	-0.2980	-0.3047	2.23
$C_{\eta_{2\,\alpha}}$	0.0258	0.0264	2.49
$C_{\eta_{2\,q}}$	0.0116	-0.0817	-804.52
$C_{\eta_{2\,\delta}}$	-0.0011	-0.0011	1.11
$C_{z_{\eta_2}}$	0.3060	0.4012	31.11
$C_{z_{\dot{\eta_2}}}$	1.0300	-4.1623	-504.11
$C_{m_{\eta_2}}$	-0.0250	-0.0690	176.01
$C_{m_{\dot{\eta_2}}}$	1.2300	0.8961	-27.15

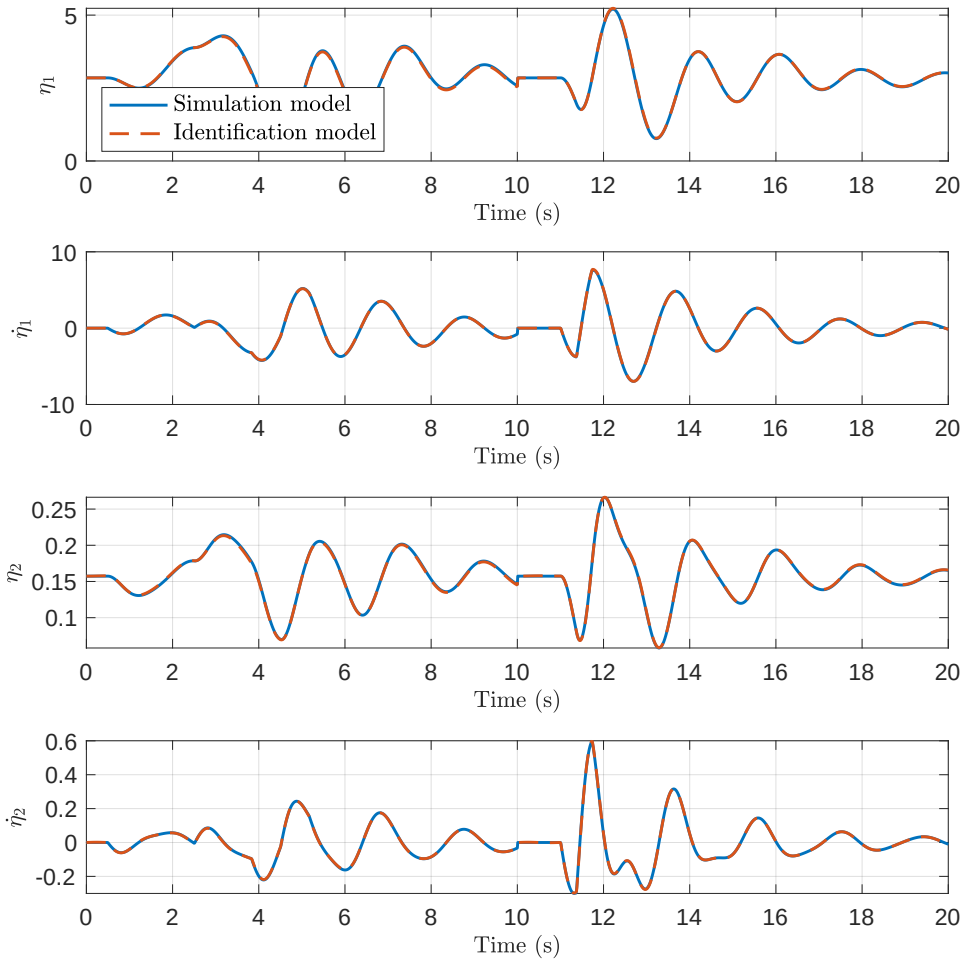

Figure 17: Very flexible model as simulation model, flexible aircraft with 2 modes as identification model - modal displacemnts

5.4 Including force loads as measured ouputs

Despite the good agreement between the responses identified and original model obtained in the previous results, many stability and control derivatives presented relatively large percentage errors during the identification procedure. During identification, a large correlation was observed between several parameters. To improve identification, we decided to add new measurement outputs: the rigid-body force Z (or, equivalently, the acceleration $\dot{w}$), and the rigid-body moment M (or, equivalently, the angular acceleration $\dot{q}$). The results for the simulation models C3 and C4, using the two-mode identification model, are resumed in Tables 11 and 12. An important improvement of most stability and control derivatives. Only five derivatives exhibit errors larger than 10%.

Table 11: Comparison of Nominal and Identified Parameters - C3 aircraft - 2 modes identification model measuring forces as outputs

Parameter	Nominal Value	Identified Value	Percentual Error (%)
C_{z0}	-0.3400	-0.3407	0.21
C_{z_α}	-2.9221	-2.9157	-0.22
C_{z_q}	14.7000	14.2570	-3.01
$C_{z_{\delta_e}}$	-0.0076	-0.0076	0.05
C_{m_0}	-0.2520	-0.2519	-0.06
C_{m_α}	-1.6616	-1.6515	-0.61
C_{m_q}	-34.7500	-33.5513	-3.45
$C_{m_{\delta_e}}$	-0.0450	-0.0450	-0.05
$C_{\eta_{1\,\alpha}}$	-0.0149	-0.0151	1.54
$C_{\eta_{1\,\delta}}$	-0.0002	-0.0002	-0.53
$C_{z_{\eta_1}}$	-0.0288	-0.0290	0.54
$C_{z_{\dot{\eta_1}}}$	-0.0848	-0.0835	-1.52
$C_{m_{\eta_1}}$	-0.0321	-0.0320	-0.25
$C_{m_{\dot{\eta_1}}}$	-0.1590	-0.1582	-0.47
$C_{\eta_{1\,q}}$	-0.0949	-0.0892	-5.98
$C_{\eta_{1\,\eta_1}}$	0.0001	0.0001	-13.55
$C_{\eta_{1\,\dot{\eta_1}}}$	-0.0004	-0.0004	-4.88
$C_{\eta_{1\,\eta_2}}$	-0.0001	0.0002	-308.54
$C_{\eta_{2\,\eta_1}}$	0.0042	0.0042	-0.13
$C_{\eta_{2\,\eta_2}}$	-0.0922	-0.0916	-0.60
$C_{\eta_{1\,\dot{\eta_2}}}$	-0.0002	-0.0009	377.32
$C_{\eta_{2\,\dot{\eta_1}}}$	0.0087	0.0089	1.84
$C_{\eta_{2\,\dot{\eta_2}}}$	-0.2980	-0.3010	1.01
$C_{\eta_{2\,\alpha}}$	0.0258	0.0267	3.75
$C_{\eta_{2\,q}}$	0.0116	0.0343	195.76
$C_{\eta_{2\,\delta}}$	-0.0011	-0.0011	-0.22
$C_{z_{\eta_2}}$	0.3060	0.3118	1.89
$C_{z_{\dot{\eta_2}}}$	1.0300	1.0013	-2.79
$C_{m_{\eta_2}}$	-0.0250	-0.0322	28.96
$C_{m_{\dot{\eta_2}}}$	1.2300	1.2150	-1.22

Table 12: Comparison of Nominal and Identified Parameters - C4 aircraft - 2 modes identification model measuring forces as outputs

Parameter	Nominal Value	Identified Value	Percentual Error (%)
C_{z0}	-0.3400	-0.3411	0.32
C_{z_α}	-2.9221	-2.9485	0.90
C_{z_q}	14.7000	13.0068	-11.52
$C_{z_{\delta_e}}$	-0.0076	-0.0076	0.05
C_{m_0}	-0.2520	-0.2514	-0.24
C_{m_α}	-1.6616	-1.6777	0.97
C_{m_q}	-34.7500	-36.4293	4.83
$C_{m_{\delta_e}}$	-0.0450	-0.0449	-0.12
$C_{\eta_{1\,\alpha}}$	-0.0149	-0.0150	0.61
$C_{\eta_{1\,\delta}}$	-0.0002	-0.0002	0.69
$C_{z_{\eta_1}}$	-0.0288	-0.0291	0.91
$C_{z_{\dot{\eta_1}}}$	-0.0848	-0.0698	-17.74
$C_{m_{\eta_1}}$	-0.0321	-0.0324	0.90
$C_{m_{\dot{\eta_1}}}$	-0.1590	-0.1440	-9.42
$C_{\eta_{1\,q}}$	-0.0949	-0.1108	16.76
$C_{\eta_{1\,\eta_1}}$	0.0001	0.0001	16.91
$C_{\eta_{1\,\dot{\eta_1}}}$	-0.0004	-0.0003	-35.42
$C_{\eta_{1\,\eta_2}}$	-0.0001	-0.0003	288.89
$C_{\eta_{2\,\eta_1}}$	0.0042	0.0042	0.61
$C_{\eta_{2\,\eta_2}}$	-0.0922	-0.0930	0.92
$C_{\eta_{1\,\dot{\eta_2}}}$	-0.0002	0.0000	-108.78
$C_{\eta_{2\,\dot{\eta_1}}}$	0.0087	0.0093	7.11
$C_{\eta_{2\,\dot{\eta_2}}}$	-0.2980	-0.3041	2.05
$C_{\eta_{2\,\alpha}}$	0.0258	0.0266	3.04
$C_{\eta_{2\,q}}$	0.0116	-0.0543	-568.09
$C_{\eta_{2\,\delta}}$	-0.0011	-0.0011	1.14
$C_{z_{\eta_2}}$	0.3060	0.3124	2.09
$C_{z_{\dot{\eta_2}}}$	1.0300	1.0300	0.00
$C_{m_{\eta_2}}$	-0.0250	-0.0213	-14.76
$C_{m_{\dot{\eta_2}}}$	1.2300	1.2198	-0.83

5.5 Using structural displacements and accelerations as measured outputs

One of the major limitations of the tests presented in the previous sections is that they assume one can measure the modal coordinates η_i and their time-derivatives $\dot{\eta}_i$. Clearly, they cannot be measured directly. Thus, this section tests measuring displacements and accelerations along the airplane.

The relative displacements are real measurable quantities that directly depend on the modal shapes and displacements, as presented in Equation 4. This type of measurement can be obtained through visual tracking, using strategically positioned cameras (for example, at the wing root) and measuring the deflection of marked points at other stations in the wing, as in the research conducted by [11]. Ref. [10] do not provide specific data on the modal shapes but a graphical representation of them, with the sensors positioned at the quarter-chord of the wing, as shown in Figures 18 and 19. Since the analysis is focused on two symmetric elastic modes, information on the relative deflections in the z axis is sufficient for a complete description of the problem.

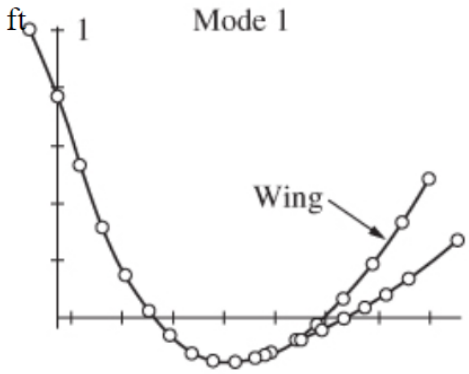

Figure 18: First elastic mode. Source: [12]

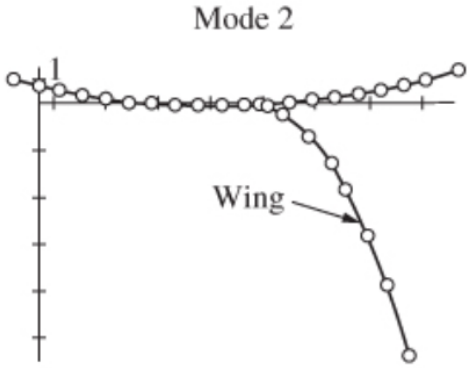

Figure 19: Second elastic mode. Source: [10]

Using software for point acquisition, it is possible to obtain estimated data of the modal shapes at each station on the wing. Thus, the simulation model is fed and identification can be carried out through the relative displacements. The points obtained are presented in Table 13, where l_{cg_i} represents the arm relative to the CG of each sensor, ϕ_1 the modal displacement relative to mode 1, and ϕ_2 the modal displacement relative to the second elastic mode.

Table 14 presents the values of the derivatives obtained considering displacement sensors.

Table 13: Values of the modal shapes and the arm relative to the CG at the wing's sensor stations in meters

l_{cg_i}	-13.289	-10.668	-8.199	-5.669	-3.109	12.131	23.119	16.581
ϕ_1	0.148	0.100	0.055	0.019	-0.043	-0.019	0.234	0.046
ϕ_2	-0.020	0.062	0.120	0.176	0.282	0.283	0.299	0.287

Table 14: Comparison of Nominal and Identified Parameters - 2 modes identification model

Parameter	Nominal Value	Identified Value	Percentual Error (%)
C_{z0}	-0.3400	-0.3412	0.36
C_{z_α}	-2.9221	-2.9414	0.66
C_{z_q}	14.7000	12.8276	-12.74
$C_{z_{\delta_e}}$	-0.0076	-0.0076	0.43
C_{m_0}	-0.2520	-0.2511	-0.34
C_{m_α}	-1.6616	-1.6725	0.66
C_{m_q}	-34.7500	-36.0941	3.87
$C_{m_{\delta_e}}$	-0.0450	-0.0449	-0.17
$C_{\eta_{1\alpha}}$	-0.0149	-0.0147	-1.35
$C_{\eta_{1\delta}}$	-0.0002	-0.0002	1.73
$C_{z_{\eta_1}}$	-0.0288	-0.0293	1.74
$C_{z_{\dot{\eta}_1}}$	-0.0848	-0.0688	-18.87
$C_{m_{\eta_1}}$	-0.0321	-0.0326	1.60
$C_{m_{\dot{\eta}_1}}$	-0.1590	-0.1453	-8.64
$C_{\eta_{1q}}$	-0.0949	-0.1089	14.80
$C_{\eta_{1\eta_1}}$	0.0001	0.0001	42.30
$C_{\eta_{1\dot{\eta}_1}}$	-0.0004	-0.0005	27.55
$C_{\eta_{1\eta_2}}$	-0.0001	-0.0007	699.77
$C_{\eta_{2\eta_1}}$	0.0042	0.0043	1.51
$C_{\eta_{2\eta_2}}$	-0.0922	-0.0939	1.82
$C_{\eta_{1\dot{\eta}_2}}$	-0.0002	0.0054	-2824.69
$C_{\eta_{2\dot{\eta}_1}}$	0.0087	0.0085	-2.49
$C_{\eta_{2\dot{\eta}_2}}$	-0.2980	-0.2879	-3.39
$C_{\eta_{2\alpha}}$	0.0258	0.0263	2.02
$C_{\eta_{2q}}$	0.0116	-0.0332	-386.18
$C_{\eta_{2\delta}}$	-0.0011	-0.0011	1.01
$C_{z_{\eta_2}}$	0.3060	0.3176	3.78
$C_{z_{\dot{\eta}_2}}$	1.0300	1.0067	-2.26
$C_{m_{\eta_2}}$	-0.0250	-0.0164	-34.60
$C_{m_{\dot{\eta}_2}}$	1.2300	1.1512	-6.41

The accelerations can also me measured at a point x_j, y_j and z_j of the aircraft as:

$$a_z^j = -\dot{w} + qu - l_{cg_j}\dot{q} + \sum_{i=1}^{\infty} \phi_i(x_j, y_j, z_j)\ddot{\eta}_i(t). \tag{19}$$

Table 15 presents the values of the derivatives considering measuring the acceleration at different points of the structure. There is a clear improvement in the estimation of derivatives with respect to the use of displacements.

Table 15: Comparison of Nominal and Identified Parameters - 2 modes identification model

Parameter	Nominal Value	Identified Value	Percentual Error (%)
C_{z0}	-0.3400	-0.3405	0.14
C_{z_α}	-2.9221	-2.9658	1.50
C_{z_q}	14.7000	13.0603	-11.15
$C_{z_{\delta_e}}$	-0.0076	-0.0076	0.38
C_{m_0}	-0.2520	-0.2516	-0.18
C_{m_α}	-1.6616	-1.6782	1.00
C_{m_q}	-34.7500	-36.5507	5.18
$C_{m_{\delta_e}}$	-0.0450	-0.0449	-0.13
$C_{\eta_{1\,\alpha}}$	-0.0149	-0.0151	1.30
$C_{\eta_{1\,\delta}}$	-0.0002	-0.0002	-0.52
$C_{z_{\eta_1}}$	-0.0288	-0.0286	-0.56
$C_{z_{\dot{\eta}_1}}$	-0.0848	-0.0647	-23.75
$C_{m_{\eta_1}}$	-0.0321	-0.0324	0.83
$C_{m_{\dot{\eta}_1}}$	-0.1590	-0.1427	-10.28
$C_{\eta_{1\,q}}$	-0.0949	-0.1131	19.14
$C_{\eta_{1\,\eta_1}}$	0.0001	0.0001	1.06
$C_{\eta_{1\,\dot{\eta}_1}}$	-0.0004	-0.0003	-38.87
$C_{\eta_{1\,\eta_2}}$	-0.0001	-0.0001	27.68
$C_{\eta_{2\,\eta_1}}$	0.0042	0.0042	-1.29
$C_{\eta_{2\,\eta_2}}$	-0.0922	-0.0924	0.23
$C_{\eta_{1\,\dot{\eta}_2}}$	-0.0002	0.0004	-293.82
$C_{\eta_{2\,\dot{\eta}_1}}$	0.0087	0.0075	-13.74
$C_{\eta_{2\,\dot{\eta}_2}}$	-0.2980	-0.2973	-0.23
$C_{\eta_{2\,\alpha}}$	0.0258	0.0334	29.58
$C_{\eta_{2\,q}}$	0.0116	-0.0184	-258.54
$C_{\eta_{2\,\delta}}$	-0.0011	-0.0011	1.35
$C_{z_{\eta_2}}$	0.3060	0.3054	-0.19
$C_{z_{\dot{\eta}_2}}$	1.0300	1.0430	1.26
$C_{m_{\eta_2}}$	-0.0250	-0.0225	-9.83
$C_{m_{\dot{\eta}_2}}$	1.2300	1.2236	-0.52

6 CONCLUSIONS AND FURTHER WORK

Aviation faces challenges such as reducing pollutant emissions, leading to a trend towards aircraft with higher aspect ratios for greater efficiency and lower fuel consumption. However, this

raises concerns about flight dynamics due to the coupling between rigid and elastic modes at lower frequencies.

Research in flexible aircraft modeling, simulation, and testing has advanced significantly. At the Instituto Tecnológico de Aeronáutica (ITA), in partnership with the University of Michigan, the LNCA (Laboratory of New Concepts in Aeronautics) utilized the X-HALE prototype for these studies; see Figure 1. Validating these models is essential, making system identification a crucial tool.

For flexible aircraft, [10] provided stability derivatives for up to four flexible modes, making it the chosen model for this study. Simulations were conducted for configurations C1 (rigid body), C3 (flexible), and C4 (very flexible), using 3-2-1-1 and doublet maneuvers. Simulated data, polluted with Gaussian white noise, were used for identification considering short-period dynamics.

C1 was identified using rigid-body dynamics, leading to accurate results. Using rigid-body dynamics for C3 led to good response agreement but poor stability derivative accuracy. For C4, the identification using a rigid-body model resulted in low agreement in both response and parameter identification.

An analysis adding observation variables (and sensors) was performed for both C3 and C4 under two conditions: (1) using data from angle of attack, pitch rate, and modal displacements (and rates); (2) adding normal acceleration and angular acceleration measurements around the y-axis. The second condition successfully identified all but two of thirty derivatives.

A comparative study on deflection and acceleration sensors showed that acceleration measurements provided better parameter estimates than deflections alone. Unlike [8], this study did not fix parameters during identification and used sensors that could be practically implemented, such as deflection and acceleration sensors.

This research underscores the importance of preliminary sensor placement studies and maneuver selection to excite all relevant dynamics for accurate stability and control derivative identification.

Future work could explore identifying natural frequencies and damping factors of elastic modes without prior knowledge, using different sensors, and validating with experimental data. Additionally, extending the analysis to include other types of sensors, such as strain gauges, and applying the identification methods to real flight test data would provide further validation. Implementing criteria like Theil's inequality coefficient for validation and comparing responses in frequency domains between real and estimated models could enhance the robustness of the identification process. More complex identification models should be expected when dealing with highly flexible aircraft, assuming geometrically nonlinear structures, thus leading to challenges in modeling simplified and parametric equations for such a problem.

These efforts will pave the way for identifying the ITA X-HALE aircraft, which will be used for model validation, control design, and further development of flexible aircraft technologies.

ACKNOWLEDGMENTS

This study was financed in part by Finep and Embraer S.A. under the research project "Advanced Studies in Flight Physics and Control" - contract number 01.22.0552.00, and in part by

the *Coordenação de Aperfeiçoamento de Pessoal de Nível Superior - Brasil* (CAPES) - Finance Code 001.

7 REFERENCES

[1] Guimarães Neto, A. B., Barbosa, G. C., Paulino, J. A., et al. (2023). Flexible aircraft simulation validation with flight test data. *AIAA Journal*, 61(1), 285–304.

[2] Guimarães Neto, A. B., Cardoso-Ribeiro, F. L., and Silvestre, F. J. (2018). Applicability of geometrically-linear structural-dynamic models for the flight dynamics of arbitrarily-flexible aircraft. In *Proceedings of the 31st Congress of the International Council of the Aeronautical Sciences, ICAS 2018*. p. 14.

[3] Jategaonkar, R. (2015). *Flight Vehicle System Identification*. AIAA.

[4] Tischler, M. B. and Remple, R. K. (2012). *Aircraft and Rotorcraft System Identification*. AIAA.

[5] Schwanz, R. and Wells, W. (1974). Estimation of elastic aircraft parameters using the maximum likelihood method. *Parameter Estimation Techniques and Applications in Aircraft Flight Testing, H. Rediess, ed., no. TN D-7647, NASA, Edwards, CA*, 337–358.

[6] Zerweckh, S., Von Flotow, A., and Murray, J. (1990). Flight testing a highly flexible aircraft. *Journal of Aircraft*, 27(4), 342–349.

[7] Silva, B. G. d. O. and Monnich, W. (2012). System identification of flexible aircraft in time domain. *AIAA journal*.

[8] Majeed, M. and Kar, I. N. (2012). Identification of aerodynamic derivatives of a flexible aircraft using output error method. In *Applied Mechanics and Materials*, vol. 110. Trans Tech Publ, pp. 5328–5335.

[9] Pfifer, H. and Danowsky, B. P. (2016). System identification of a small flexible aircraft-invited. In *AIAA Atmospheric Flight Mechanics Conference*. p. 1750.

[10] Waszak, M. R. and Schmidt, D. K. (1988). Flight dynamics of aeroelastic vehicles. *AIAA journal*, 25(6), 563–571.

[11] Sanches, A. C. (2019). Stereo vision-based technique to measure in-flight wing displacement of a very flexible aircraft.

[12] Waszak, M. R., Davidson, J. B., and Schmidt, D. K. (1987). A simulation study of the flight dynamics of elastic aircraft. volume 1: Experiment, results and analysis. Tech. rep., NASA. NASA-CR-4102.

COPYRIGHT STATEMENT